The International Journal of Advanced Manufacturing Technology (2023) 127:3979–3987
https://doi.org/10.1007/s00170-023-11708-3

ORIGINAL ARTICLE

Influence of extrusion method on the microstructure and mechanical properties of formed magnesium alloy tubes

Hui Zhao[1] · Hong-jun Hu[1] · Peng-cheng Liang[1]

Received: 24 October 2022 / Accepted: 4 June 2023 / Published online: 22 June 2023

Abstract
In this work, a tube extrusion-shear-expanding (TESE) process was proposed to develop a high-performance magnesium alloy thin-walled tube, and then a comparison was made with the direct extrusion (DE) process. The microstructure and mechanical properties of magnesium alloy tubes under different processes were tested and analyzed. Numerical simulations were conducted by using DEFORM^{TM}-3D software to predict the effective stresses, forming loads, and effective strains during the forming of magnesium alloy tubes. Compared with DE process, the TESE process with high effective stresses, effective strains, and forming loads generates a severe plastic deformation of the tube, leading to a more obvious grain refinement effect on the fabricated tube with a tensile strength of around 293 MPa and an elongation of around 15%. The results show that the TESE process has obvious advantages. The critical shear force and dynamic recrystallization further refine the grains and weaken the basal texture strength. The comprehensive performance of magnesium alloy tube is improved.

Keywords Magnesium alloy · Numerical simulation · Grain refinement · Mechanical property

1 Introduction

Magnesium alloys have high specific strength, specific stiffness, electrical conductivity, and processing properties [1–4], which are widely used in aerospace, communication equipment, and other fields [5, 6]. However, magnesium alloy displays a poor plasticity at room temperature because of its unique hexagonal close-packed (HCP) crystal structure [7, 8]. Thus, secondary processing is usually used at high temperature to improve its plasticity, including rolling [9–11], casting [12, 13], and extrusion [14–16].

Currently, improving the plasticity of magnesium alloy tubes by extrusion deformation has become the main trend of various scholars. Che et al. [17] used rotating backward extrusion (RBE) to produce AZ80 magnesium alloy cup-shaped. The results show that the RBE process can improve the fluidity and equivalent strain of the metal of the cup compared with the conventional backward extrusion (CBE) process. The RBE process can significantly refine the grains, increase the proportion of dynamic recrystallization, and aggravate the fragmentation and refinement of the second phase. Chen et al. [18] developed a novel type of composite die to achieve continuous cyclic extrusion deformation of AZ31 magnesium alloy with variable cross-section. After three cycles of deformation, the grain orientation of AZ31 magnesium alloy exerted a directional transformation, leading to the refinement of average grain sizes of the upper and lower ends to 6.1 μm and significant improvement of the microhardness and tensile strength in both horizontal and axial directions. Zhang et al. [19] used DEFORM-3D software to simulate the reverse extrusion forming of AZ31 magnesium alloy and explored the influence of extrusion temperature, extrusion speed, and die angle on the reverse extrusion forming process and obtained the best process parameters. Lei et al. [20] used DEFORM-3D software to simulate the wide spreading and split extrusion process of large diameter AZ31 magnesium alloy tube, and the optimum process parameters were determined. Through the above scholars' research on extrusion forming, it is found that the extrusion forming process can refine the grains of magnesium alloy. The combination of numerical simulation and extrusion process can optimize the die structure and extrusion process parameters and seek the best extrusion process conditions, so as to improve the quality of extrusion products and reduce the experimental cost.

✉ Hong-jun Hu
hhj@cqut.edu.cn

[1] Materials Science and Engineering College, Chongqing University of Technology, No. 69 Hongguang Road, Banan town, Chongqing 400050, China

In general, although constant speed and temperature were adopted during the preparation of magnesium alloy tubes, the direct extrusion (DE) process may result in small plastic deformation, uneven grain size, and poor mechanical properties in the prepared samples.

Therefore, a direct extrusion and continuous multiple shearing was combined to prepare magnesium alloy profiles in our previous work [21–23]. Compared with direct extrusion, extrusion shearing could generate severe plastic deformation, a refinement of grain size, and an improved yield strength of the magnesium alloy.

The present work proposed a tube-extrusion-shear-expanding (TESE) process to improve the microstructure of magnesium alloy tubes and improve the quality of tubes. In the TESE process, local back pressure and shear stress are applied to the material at the corners to further refine the grain sizes and improve the machinability and strength of the magnesium alloy. The comparison between direct extrusion (DE) and TESE processes was conducted, and DEFORM^{TM}-3D finite element software was employed to reveal the evolution of effective stress of billets, forming loads, and effective strains during the tube different extrusion methods. The microstructure, texture strength, and mechanical properties of magnesium alloy tubes prepared by different extrusion methods were analyzed and compared.

2 Experimental

2.1 Materials

The experimental material was commercial AZ31 magnesium alloy with the elemental mass fractions shown in Table 1. The experimental equipment used multi-cylinder servo synchronous extruder, the maximum force of 2500 KN. Before the extrusion experiment, the magnesium alloy billet was processed to a tube sample with a length of 80 mm, an outer diameter of φ40 mm, and an inner diameter of φ20 mm. The magnesium alloy tube was polished with SiC sandpaper to remove surface oxides and impurities. The heating rod was used to preheat the mold and billet. The thermocouple thermometer was used to monitor the temperature of the billet every five minutes. When the temperature reached the specified temperature, the extrusion was performed. The extrusion temperature was 440 °C, and the extrusion speed was 4mm/s.

2.2 FEM simulation

In this paper, the finite element numerical simulation method is used to analyze the forming conditions and multi-physical fields in each stage of the billet forming process. Due to the symmetrical nature of the tube-forming process, a 1/2 model was used for the simulation to increase the rate of calculation, the specific parameters of which are shown in Table 2. Figure 1 shows schematic diagrams of the die structures of the TESE and DE processes. The die is mainly composed of a punch, container, magnesium billet, die, and mandrel.

2.3 Microstructural characterization and mechanical testing

The microstructures were analyzed using an optical microscopy (OM) under different processes. The samples were polished and corroded by etching solution (3g picric acid + 20 ml acetic acid + 50 ml ethanol + 20 ml distilled water). The microstructure of the samples prepared by different processes was observed by OM (Leica DMI5000M).

The mechanical properties of the tubes were tested using tensile testing and hardness testing. Tensile test samples were taken by wire cutting, with a sample size of 30 mm × 2 mm × 1 mm, as shown in Fig. 2a. Tensile tests were carried out using an MTS universal tensile tester at a room temperature of 20 °C at a rate of 0.5 mm/min. Fracture analysis was carried out using SEM immediately after stretching. The hardness of the tubes was tested for different processes using the HVS-100Z automatic turret digital

Table 2 FEM simulation parameters

Name	Parameter
Length of the tube blank (mm)	80
Inner diameter of AZ31 (mm)	20
Outer diameter of AZ31 (mm)	40
Preheated temperature of tube blank (°C)	440
The extrusion velocity (mm/s)	4
Number of mesh	30000
Mesh density type	Relative
Thermal conductivity between billet and die (N/(°C·s·mm))	11
Friction coefficient	0.25
Simulation type	Lagrangian incremental

Table 1 Chemical composition of AZ31 magnesium alloy (wt%)

Material	Al	Zn	Mn	Cu	Fe	Si	Mg
AZ31	2.80	0.70	>0.20	0.01	0.05	0.08	Balance

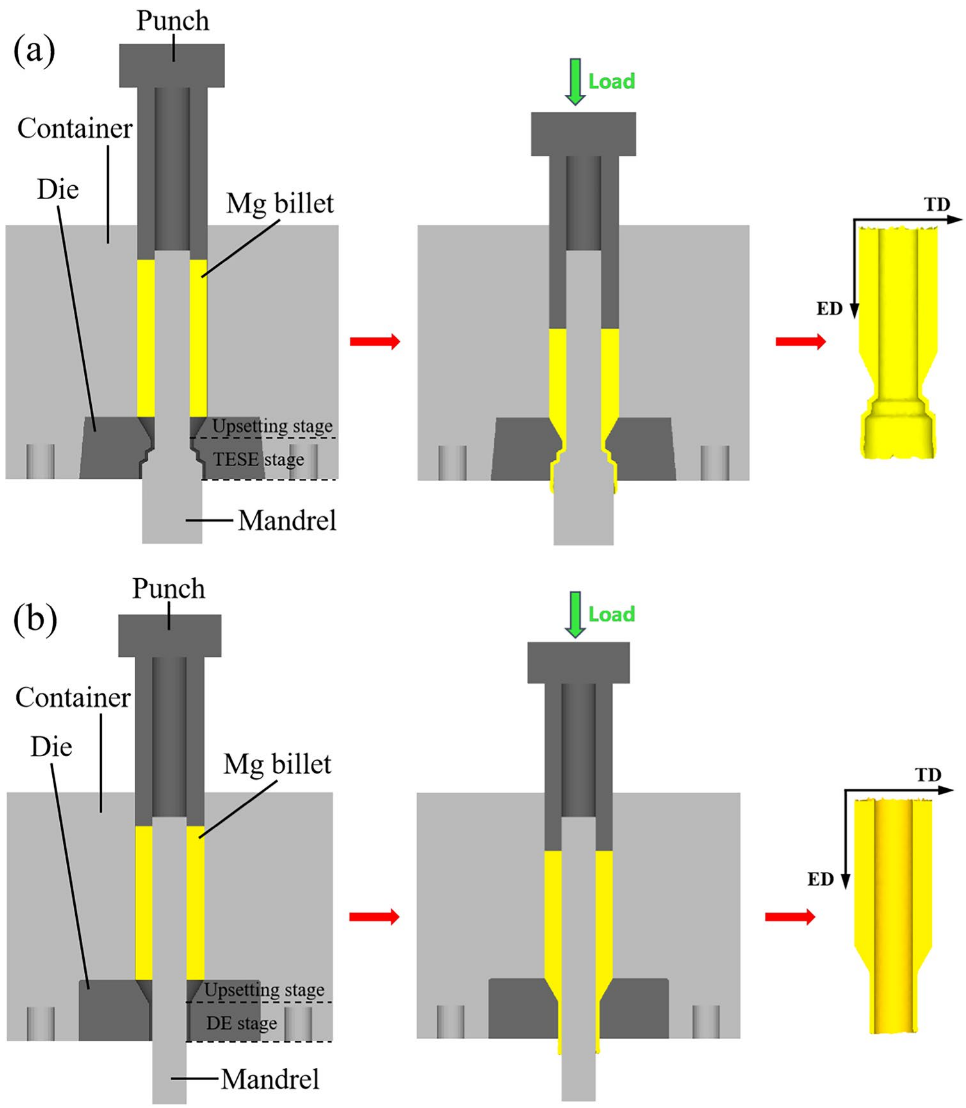

Fig. 1 Schematic diagram of the die structures of **a** TESE process and **b** DE process

display microhardness tester. Each sample was tested using ten points, and the average was obtained by removing the maximum and minimum values. The hardness test was loaded with a load of 100 g and a holding time of 10 s.

The texture of the samples was analyzed by X-ray diffractometer (XRD). The texture of the formed tube was detected by a PANalytical Empyrean X-ray Diffractometer. The Cu target was used, the acceleration voltage was 40 Kv, the current was 40 mA, and the scanning step was 0.02°. Samples were taken as shown in Fig. 2b, and XRD samples were polished with SiC sandpaper and soaked in alcohol solution for testing.

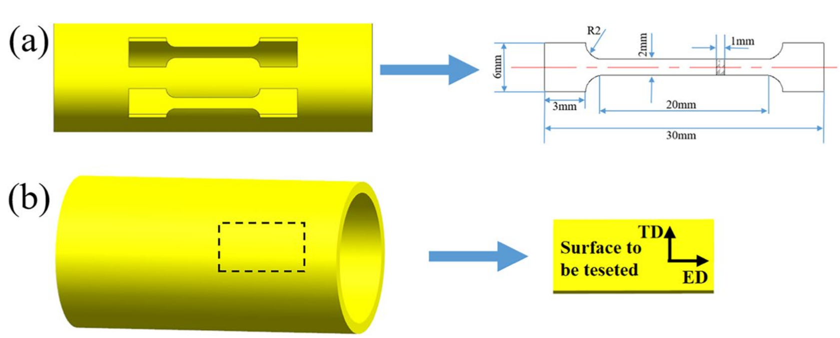

Fig. 2 **a** Tensile sample. **b** XRD sample

3 Results and discussion

3.1 FEM analysis

3.1.1 Evolution of effective stress at different processes

Figure 3 shows the stress evolution at different stages of the TESE and DE processes at a preheating temperature of 440°C. Under the action of the extrusion rod, the forming of the tube experienced upsetting stage, TESE stage, and DE stage respectively. From the overall distribution of the equivalent stress of the tube, the effective stress at both ends is greater than the middle part. The maximum effective stress of the tube blank appears in the upper part. Because the upper part of the tube blank is directly affected by the extrusion rod, the stress value is larger. As shown in Fig. 3b and c, the upsetting deformation of the billet was completed to enter the shear zone. The larger the shear stress generated in the shear zone leads to an increased deformation resistance. Meanwhile, the billet was also hindered by the corner, showing an irregular stress distribution of TESE stage and a maximum stress of approximately 28.5 MPa. It can be seen from Fig. 3f and g, when the billet entered into the DE stage, due to the constraints of the mold, the deformation is small, and the maximum stress is about 17.6 MPa.

3.1.2 Load–stroke variation for different TESE processes

Figure 4 shows the forming load curves of magnesium alloy tubes during the DE and TESE processes. It can be seen that the forming loads during the two deformation process both gradually increased with the increase of the strokes. Besides, the loads gradually increased with the plastic deformation of the billet under the extrusion forces during the upsetting forging

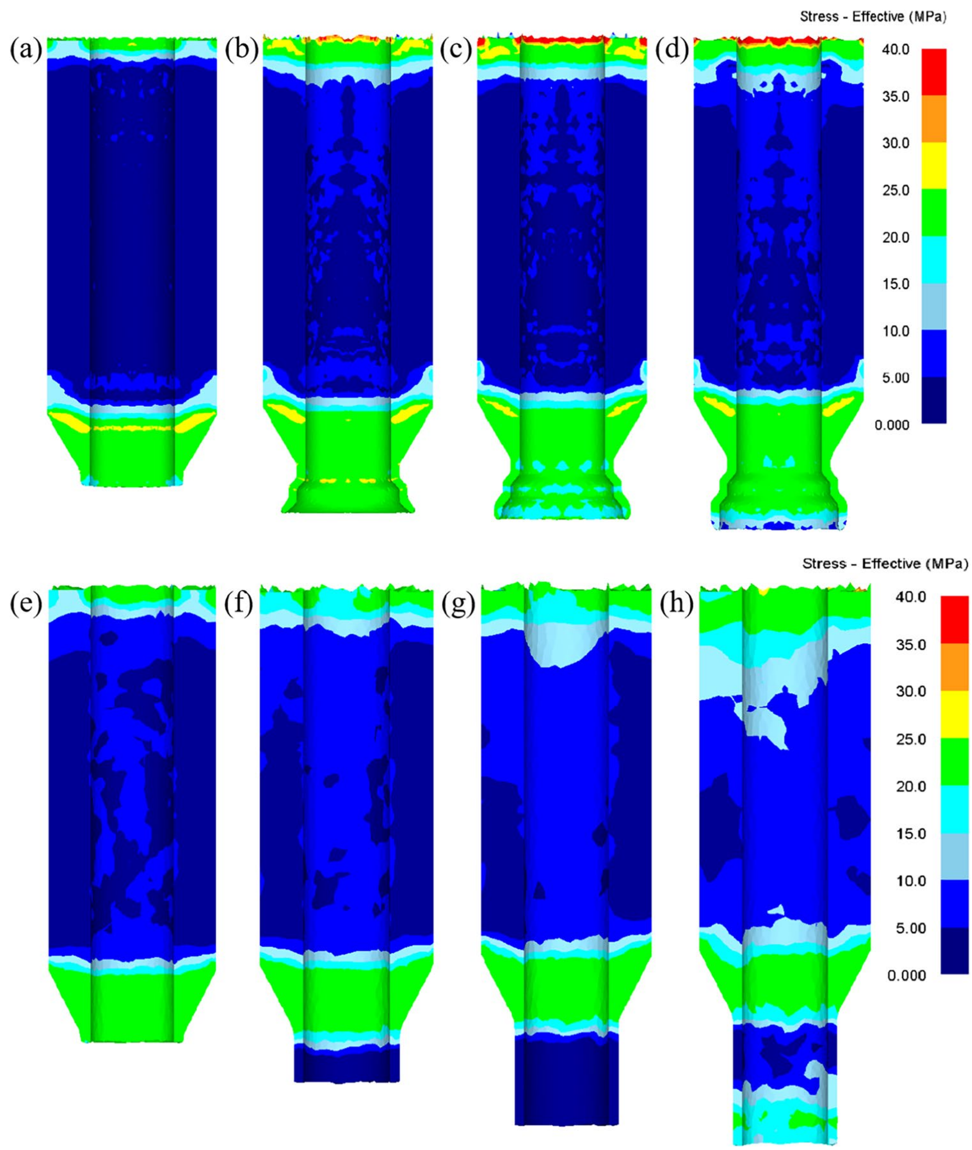

Fig. 3 Stress changes in tube billets during forming by the TESE and DE processes: **a**, **e** upsetting stage, **b**, **c** TESE stage, **f**, **g** DE stage, **d**, **h** sizing stage

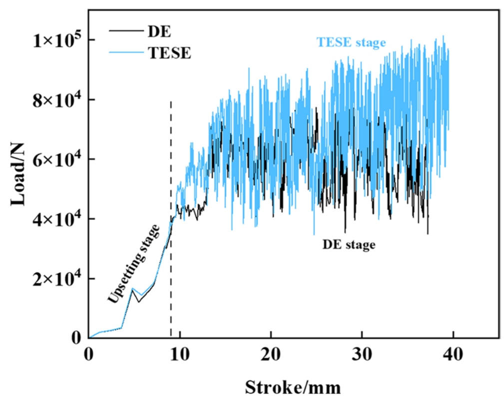

Fig. 4 Load–stroke curves of formed tubes for different processes

stage of two processes. As the extrusion process proceeded, the billet underwent the TESE process, resulting in a further plastic deformation and an increased extrusion force rapidly under the extrusion forces and die corner shear. Compared with the TESE process, the billet underwent the DE stage with a relatively low extrusion force, leading to a lower load in the DE process. The maximum forming load during the TESE process decreased by 57% from 9.3×10^4 N to 4×10^4 N.

3.1.3 Effective strain evolution of formed tubes under different processes

To further investigate the distributions of the effective strains of the magnesium alloy tube during the TESE process, three different points at the bottom of the tube were selected by point tracing to investigate the distributions of the effective strains of magnesium alloy tube during the TESE process. The effective strain values of the DE process firstly increased to a stable state and then continued to increase, while that of the TESE process gradually increased with the progress of extrusion deformation. As shown in Fig. 5b and d, the ends of the formed tube displayed a much larger effective strain values than the middle, indicating that both two ends were the main deformation areas. The upper end of the tube with direct contact with the punch was subjected to extrusion pressure, leading to an increase in the effective strain values. The lower end was subjected to different die configurations, resulting in a severe plastic deformation and an increase in the equivalent value. In addition, the effective strain on the tube surface with two deformation methods exhibited quite different distribution. The forming process of TESE achieved a larger effective strain and a wider area of plastic deformation than DE.

Fig. 5 Strain evolution of tubes under different processes: **a–b** DE and **c–d** TESE

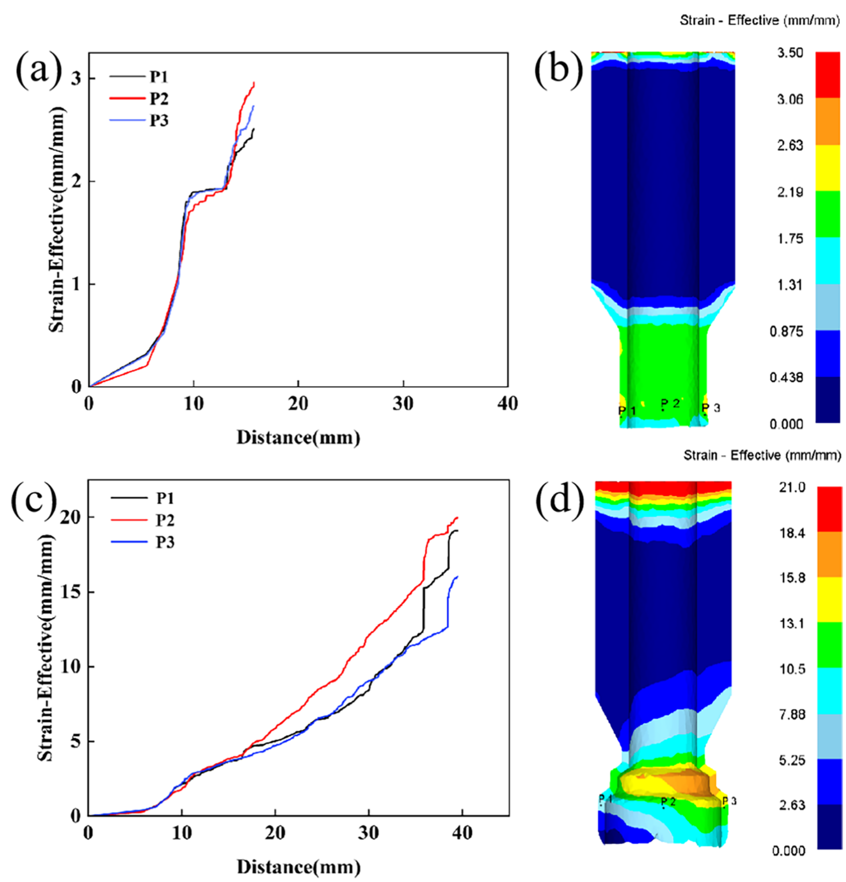

3.2 Microstructures

The cross-sections of the tubes prepared via the TESE and DE processes were observed to investigate the influences of formation process on their microstructures. As shown in Fig. 6a, the average grain size of the initial billet was approximately 59.88 μm. Figure 6b shows the microstructures of the sections in the DE-formed tube. As shown in Fig. 6b and c, the grain sizes were significantly refined with the plastic deformation during the DE and TESE processes. The deformation resulted in the breakage of the original grains and the formation of new grains. After a series of TESE process, the grains were obviously refined but with a low uniform distribution, and some large grain was still visible, which may be due to the growth of some grains to form equiaxed grains after dynamic recrystallization at a higher temperature. Figure 6c shows the cross-sectional microstructure of a tube formed by the TESE process. It can be seen that the grain size exhibited a better uniformity than that formed by the DE process. Moreover, a larger deformation volume of the TESE process allowed for more recrystallized cores per unit volume when dynamic recrystallization occurred. Compared with the DE process, the higher degree of dynamic recrystallization in the TESE process resulted in a formed tube with more equiaxed crystals and finer and more uniform grains with an average grain size of approximately 7.07 μm.

3.3 Macro-texture of magnesium alloy tubes formed by different processes

During the plastic machining of the metal, the formation of texture exerted great influence on the properties of the formed products. During the extrusion of magnesium alloy tube, the billet was subjected to the plastic deformation under the stress with a basal slip is as the main form, and the grain (0002) plane in the billet would be inclined to the direction of the principal stress axis (ED direction). Figure 7 shows the distribution of macroscopic texture in magnesium alloy tubes prepared via the DE and TESE processes with the same process parameters [24]. As can be seen from Fig. 7a, the distributions of the (0002) basal textures of the DE-formed tube indicated that the basal plane of most grains was parallel to the extrusion direction (ED), which was typical of the basal textures of magnesium alloys. As can be seen from Fig. 7b, the distributions of the (0002) basal texture in the TESE-formed tube suggested that some grains were still parallel to the ED direction. However, the orientation of the grains was significantly deflected compared with that of Fig. 7a, and the maximum polar density value dropped from 40.3 to 13.6, leading to a reduced strength of the textures. The introduction of shear angle made the magnesium alloy billet to be subjected to shear stress during the forming process, leading to an inclined overall force. Most grains would not completely tilt to the direction of compression stress during the slip process

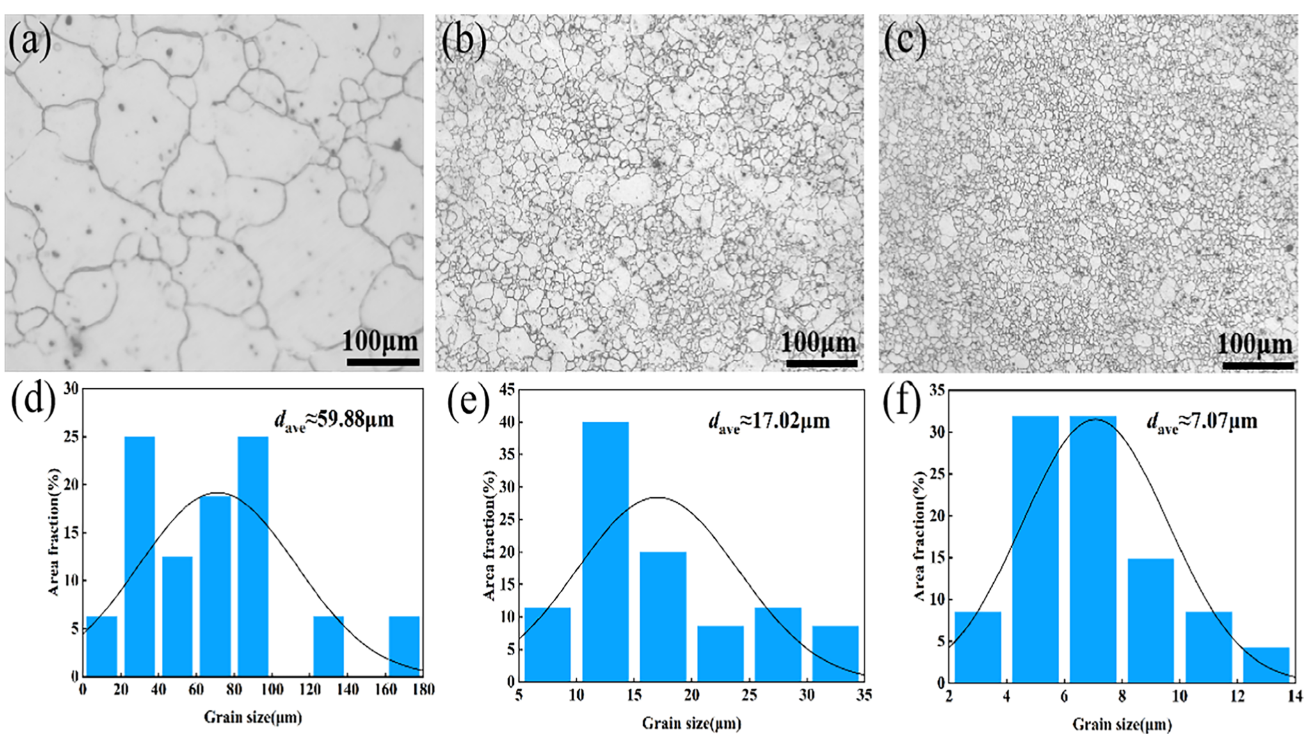

Fig. 6 Microstructure of formed tubes under different processes: OM diagram of (**a**, **b**, **c**) and grain size distribution of (**d**, **e**, **f**)

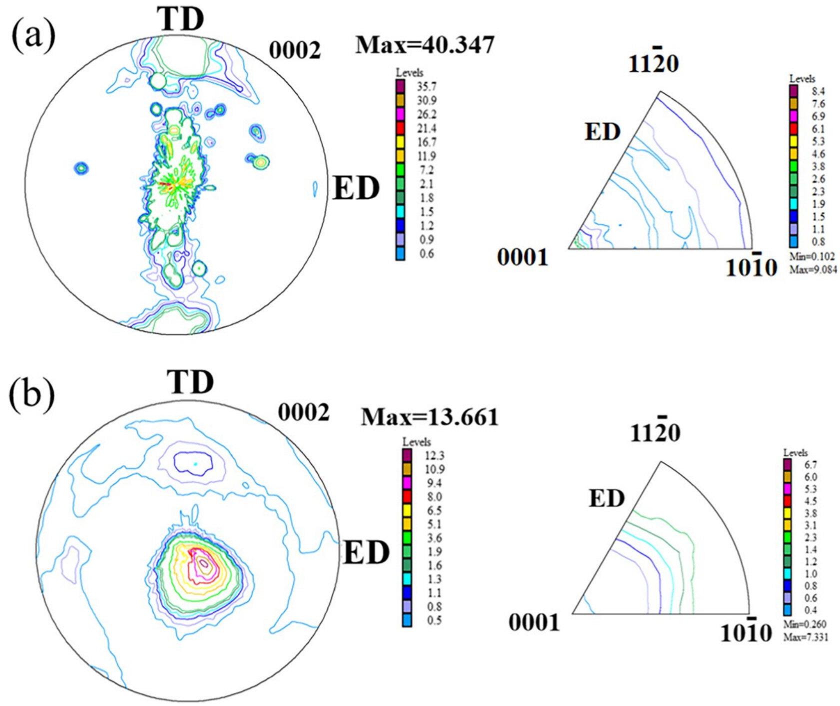

Fig. 7 Texture of formed tubes by different processes: **a** DE and **b** TESE

due to the existence of shear stress, resulting in the change of grain orientation and the decrease of texture strength.

3.4 Mechanical properties

3.4.1 Tensile tests

As an important indicator of mechanical properties of metal material, tensile properties of the tubes prepared with DE and TESE processes were determined. Figure 8 a and b show the stress–strain curves and tensile property parameters. Compared with the DE process, the magnesium alloy tubes prepared with the TESE process exhibited greatly improved mechanical properties. The tensile strength of the formed tubes under two different processes is about 226 MPa and 293 MPa, respectively. In addition, the 15 % elongation of the TESE tube is better than that of the DE tube:

$$\sigma = \sigma_0 + \mathrm{k}_0 d^{-\frac{1}{2}} \tag{1}$$

where σ is the material yield strength (MPa), σ_0 is the single crystal yield strength (MPa), k_0 is the constant, and d is the average grain size (μm).

Based on the Hall–Petch formula (Eq. 1) [25], the yield strength of the material was inversely proportional to the grain size. Due to the dynamic recrystallization of the magnesium alloy grains prepared by the TESE process, the grains were refined and homogenized significantly, leading to an increase in the number of grain boundaries within a certain range. When the deformation occurred, the grain boundary appeared to prevent dislocation slips, resulting in a dislocation accumulation at the grain boundaries and an increase of the strength.

Tensile fractures of the tubes were observed to comprehensively analyze the difference of mechanical property of

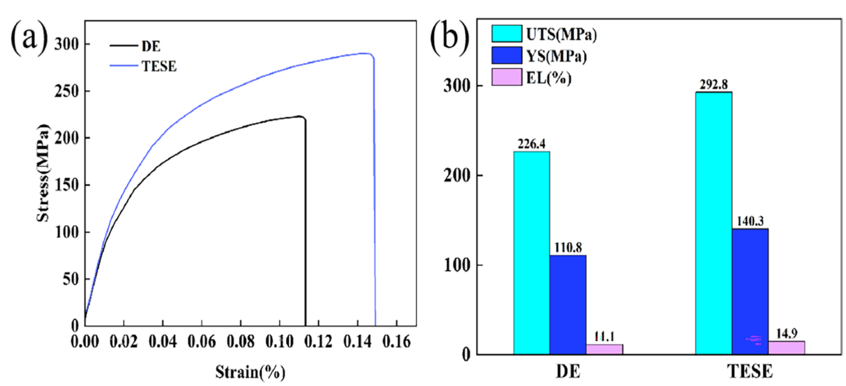

Fig. 8 **a** Tensile stress–strain curves of formed tubes for different processes. **b** Tensile properties of formed tubes for different processes

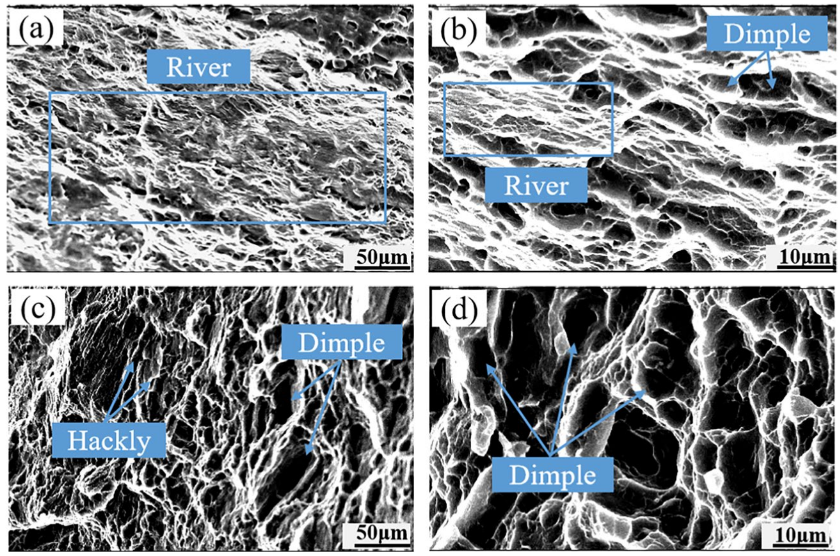

Fig. 9 Tensile fracture morphology of formed tubes prepared by different processes: **a**–**b** DE and **c**–**d** TESE

the magnesium alloy tubes prepared via the DE and TESE processes. The fracture mode is generally determined by the fracture morphology. Figure 9 a and b show the fracture patterns of the tube formed via the DE process, suggesting a relatively flat fracture at a low magnification, and an unraveling fracture with a stepped pattern at a high magnification. The fracture was split along a certain grain surface under a tensile stress, and the surface of the fracture was generally a low-index grain surface. Therefore, the (0002) plane of magnesium alloys was generally the fracture resolution plane, which was also preceded by plastic deformation. A small amount of toughness nests was also observed from Fig. 9b, indicating that the DE-formed tubes was subjected to quasi-deformation fractures. Figure 9 c and d show the fracture profiles of the tube formed via the TESE process, suggesting a distinct bladed fracture with an uneven, jagged undulating feature at a low magnification, and more equiaxed tough nests at a high magnification as a result of the specimen movement along a certain slip surface under a tensile stress. Therefore, the TESE-formed tube exhibited a fracture mode of ductile fracture, and a better plasticity than the DE-formed tube based on fracture morphology.

3.4.2 Microhardness

Figure 10 shows the distribution of the cross-sectional hardness of the tubes formed by the two processes under the same process parameters. The hardness values of the magnesium alloy tube formed by the DE and TESE processes are approximately 61 HV and 75 HV, respectively. The hardness values of the tubes formed by the TESE process are significantly higher than those of the tubes formed by the DE process. The TESE process significantly improves the deformation resistance of the magnesium alloy tube surface.

4 Conclusions

(1) In this paper, magnesium alloy thin-walled tubes are prepared by numerical simulation and experiment. The grain size of the tubes formed by the TESE process is finer and more uniformly distributed than that of the DE-formed tubes.

(2) In the tube-forming process, the effective stress and effective strain are higher in the TESE process compared to the DE process, and the maximum forming load is approximately 1.2 times higher in the TESE process than in the DE process.

(3) The mechanical properties (hardness, strength, elongation) of TESE tubes are also better than those of DE tubes with a tensile strength of around 293 MPa compared to 226 MPa for DE-formed tubes. Compared with direct extrusion (DE) forming, the addition of the shear-expanding stage can effectively weaken the basal texture of the tube, promote the degree of dynamic recrystallization, and make more grains in the soft orientation.

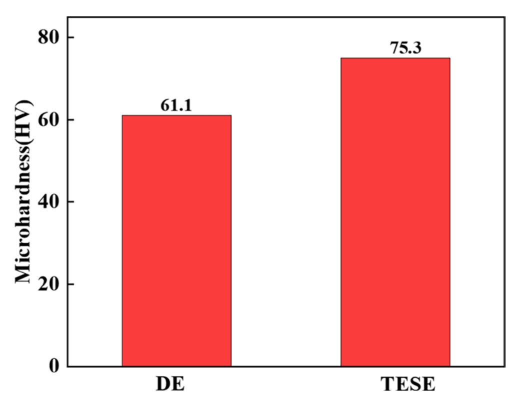

Fig. 10 Hardness of the cross-section in tubes formed by different processes

Author contributions
• Hong-jun Hu is the corresponding author of this paper who wrote the paper.
• Hui Zhao did the examples and wrote the article in this paper.
• Peng-cheng Liang did the experiments.

Data Availability The raw/processed data required to reproduce these findings cannot be shared at this time as the data also forms part of an ongoing study.

Declarations

Ethical approval No animals have been used in any experiments.

Consent to participate There is no human who has been used in any experiments.

Consent for publication The authors confirm:

That the work described has not been published before (except in the form of an abstract or as part of a published lecture, review, or thesis)
That it is not under consideration for publication elsewhere
That its publication has been approved by all co-authors, if any
That its publication has been approved (tacitly or explicitly) by the responsible authorities at the institution where the work is carried out

Competing interests The authors declare no competing interests.

References

1. Hu HJ (2013) Grain refinement of Mg−Al alloys by optimization of process parameters based on three-dimensional finite element modeling of roll casting. Trans Nonferrous Met Soc Chin 23(3):773–780
2. Sheng K, Lu LW, Xiang Y, Ma M, Wu ZQ (2019) Crack behavior in Mg/Al alloy thin sheet during hot compound extrusion. J Magnesium Alloys 7:717–724
3. Hu HJ (2013) The effects of process parameters on evolutions of thermodynamics and microstructures for composite extrusion of magnesium alloy. Adv Mater Sci Eng 2013:1–9
4. Wang JF, Peng X, Wang K, Wang Q, Gao SQ, Hu H, Pan FS (2020) Numerical simulation and experimental study on extrusion forming of ultra-large size wide thin-walled hollow magnesium alloy profiles. Chinese J Nonferrous Metals 30(12):2809–2819
5. Hu HJ, Li YY, Gong XB, Zhai ZY, Wang H, Fan JZ, Dai JL (2015) Relationships between the process conditions and microstructures evolution for extrusion-shear of magnesium alloy. Russian J Non-Ferrous Metals 56(4):455–467
6. Zhang S, Tang GH, Li Z, Jiang XK, Li KJ (2020) Experimental investigation on the springback of AZ31B Mg alloys in warm incremental sheet forming assisted with oil bath heating. Int J Adv Manuf Technol 109:535–551
7. Hu HJ (2013) The effects of special extrusion on the grain refinements of magnesium alloy. Int J Microstruct Mater Properties 8(6):436–446
8. Tian Y, Hu HJ, Zhang DF (2021) A novel severe plastic deformation method for manufacturing Al/Mg bimetallic tube. Int J Adv Manuf Technol 116:2569–2575
9. Zhang WC, Liu XT, Ma JF, Wang WK, Chen WZ, Liu YX, Yang JL (2022) Evolution of microstructure and mechanical properties of ZK60 magnesium alloy processed by asymmetric lowered-temperature rolling. Trans Nonferrous Met Soc Chin 32(9):2877–2888
10. Che B, Lu LW, Zhang JL, Zhang JH, Ma M, Wang LF, Qi FG (2022) Effects of cryogenic treatment on microstructure and mechanical properties of AZ31 magnesium alloy rolled at different paths. Mater Sci Eng A 832:142475
11. Jin GY, Cai XD, Zhou D (2021) Effect of rolling temperature on microstructure and mechanical properties of AZ61 magnesium alloy. Hot Working Technol 50(1):95–97
12. Qiu W, Yu RZ, Zhou B, Chen J, Ren YJ, Huang WY, Lu J, Li J (2020) Research progress on grain refinement of cast magnesium alloy. Foundry Technol 41(11):1077–1087
13. Wang F, Wang Y, Mao PL, Yu BY, Guo QY (2010) Effects of combined addition of Y and Ca on microstructure and mechanical properties of die casting AZ91 alloy. Trans Nonferrous Met Soc Chin 20(S2):311–317
14. Sun DH, Wang LW, Xie WK (2016) Simulation analysis on thin sheet of magnesium alloy AZ31B in the extrusion process. Forging Stamp Technol 41(1):61–66
15. Wang H, Zhang DT, Qiu C, Zhang WW, Chen DL (2022) Achieving superior mechanical properties in a low-alloyed magnesium alloy via low-temperature extrusion. Mater Sci Eng A 851:143611
16. Kang W, Lu LW, Feng LB, Lu FC, Gan CL, Li XH (2023) Effects of pre-aging on microstructure evolution and deformation mechanisms of hot extruded Mg-6Zn-1Gd-1Er Mg alloys. J Magnesium and Alloys 11(1):317–328
17. Che X, Wang Q, Dong BB, Meng M, Gao Z, Liu K, Ma J, Yang FL, Zhang ZM (2021) The evolution of microstructure and texture of AZ80 Mg alloy cup-shaped pieces processed by rotating backward extrusion. J Magnesium and Alloys 9(5):1677–1691
18. Chen P, Wang KS, Guan PL, Chen L, Wang W (2018) Effect of continuous variable cross-section on microstructure and mechanical properties of AZ31 magnesium alloy. Light Alloy Fabrication Technol 46(8):33–37
19. Zhang X, Geng DQ, Li PW, Wang P, Ding H, Cui JZ (2015) Finite element modeling of backward extrusion process for AZ31 magnesium alloy thin-wall tubes. Special Cast Nonferrous Alloys 35(9):930–933
20. Lei TF, Pan F (2019) Simulation study on SDEP extrusion process of AZ31 magnesium alloy tube with large diameter. Hot Work Technol 48(1):174–177
21. Tian Y, Hu HJ, Li Y, Zhao JX, Hong X, Jiang B, Zhang DF (2022) A continuous extrusion-shear (ES) composite process for significantly improving the metallurgical bonding and textures regulations and grain refinements of Al/Mg bimetallic composite rods. Adv Eng Mater 24(6):2200061
22. Zhao H, Hu HJ, Gan SL, Jiang B, Zhang DF (2022) Numerical simulation and experimental studies on extrusion-shear process of Al/Mg composite sheets. Special Cast Nonferrous Alloys 42(9):1114–1118
23. Hu H J, Qin X, Zhang, D F, X M (2018) A novel severe plastic deformation method for manufacturing AZ31 magnesium alloy tube. Int J Adv Manuf Technol 98:897-903
24. Chen ZH, Xia WJ, Cheng YQ, Fu DF (2005) Texture and anisotropy in magnesium alloys. Chinese J Nonferrous Metals 15(1):1–11
25. Wang Y, Wang YT, Li RD, Niu PD, Wang MB, Yuan TC, Li K (2021) Hall-Petch relationship in selective laser melting additively manufactured metals: using grain or cell size. J Central South University 28(4):1043–1057